

Probing the precision of the mitotic clock with a live-cell fluorescent biosensor

Joshua T Jones¹, Jason W Myers¹, James E Ferrell, Jr² & Tobias Meyer^{1,3}

Precise timing of mitosis is essential for high-fidelity cell duplication. However, temporal measurements of the mitotic clock have been challenging. Here we present a fluorescent mitosis biosensor that monitors the time between nuclear envelope breakdown (NEB) and re-formation using parallel total internal reflection fluorescence (TIRF) microscopy. By tracking tens to hundreds of mitotic events per experiment, we found that the mitotic clock of unsynchronized rat basophilic leukemia cells has a marked precision with 80% of cells completing mitosis in 32 ± 6 min. This assay further allowed us to observe delays in mitotic timing at Taxol concentrations 100 times lower than previous minimal effective doses, explaining why Taxol is clinically active at low concentrations. Inactivation of the spindle checkpoint by targeting the regulator Mad2 with RNAi consistently shortened mitosis, providing direct evidence that the internal mitotic timing mechanism is much faster in cells that lack the checkpoint.

Because cell duplication depends on accurate chromosome separation, mitosis is thought to be one of the most tightly regulated cellular processes. Cells have solved the fidelity problem in part by relying on a sequential processing strategy that involves timing of individual cell cycle steps and on checkpoints that monitor the completion of different cell cycle phases^{1,2}. During mitosis, the spindle checkpoint ensures the correct alignment and spindle attachment of sister chromatids^{3,4}. Failures at this critical checkpoint lead to genetic instability, which is a hallmark of cancer and is correlated with aggressive tumor behavior⁵. Techniques such as immunohistochemistry and fluorescence-activated cell sorting (FACS) analysis have provided valuable information for understanding mitotic events. However, because these methods provide snapshots of single, often synchronized cells, temporal resolution of mitosis at the single cell level is lost. Phase contrast, differential interference contrast (DIC) or fluorescence imaging of live mitotic cells eliminates some of these problems, and has been used to measure mitotic times of individual cells^{6–8}. Nevertheless, observing mitotic timing in statistically significant cell numbers remains a challenge.

Fluorescent probes are powerful tools for cell biologists and are increasingly being used in the investigation of important cellular events⁹. Because our studies suggested that light damage caused by epifluorescence or confocal illumination markedly reduces the number of cells that enter mitosis (data not shown), we set out to engineer a nonperturbing genetically encoded reporter of the timing of mitosis. To increase the number of cells that can be tracked over time and to reduce light toxicity, we have designed a system that uses wide-field TIRF microscopy and a fluorescent mitosis biosensor (FMB) for monitoring the time period between NEB, anaphase and nuclear envelope re-formation (NER) in tens to hundreds of cells per experiment. TIRF microscopy provides several advantages over confocal and other fluorescence microscopy-based assays^{10,11}. First, the lower background in

TIRF microscopy results in an improved signal-to-noise ratio and therefore increased sensitivity to small changes in membrane fluorescence^{10,11}. Second, and relevant in particular for cell cycle experiments, photobleaching and phototoxicity are greatly reduced compared to other microscopy techniques, because most of the sample is not illuminated during imaging¹¹. Therefore, imaging can be done over longer periods and with better temporal resolution without damaging the sample¹¹.

RESULTS

Design of the live-cell fluorescent biosensor

The biosensor is a fusion protein comprising three components, a reversible plasma membrane-targeting domain fused to the N terminus of enhanced yellow fluorescent protein (EYFP), that is in turn fused to the N terminus of a nuclear localization signal (NLS) (Fig. 1a). We hypothesized that a nuclear localization signal would ensure the biosensor's localization to the nucleus during the G1, S and G2 phases (interphase) of the cell cycle. Upon NEB at the onset of prometaphase, the plasma membrane-binding domain would cause the reversible translocation of the biosensor to the plasma membrane where the fluorescence could be monitored by TIRF microscopy.

We first used confocal microscopy to monitor the location of the biosensor during the cell cycle in a rat basophilic leukemia (RBL) cell line that constitutively expresses the fluorescent mitosis biosensor (RBL-FMBs). As hypothesized, the biosensor was found to reside in the nucleus during interphase, and upon NEB, the biosensor rapidly translocated to the plasma membrane (Fig. 1b and **Supplementary Movie 1** online). During telophase and cytokinesis, when the nuclear envelope reformed around the daughter chromatids, the biosensor translocated back into the nucleus where it resided until the next mitosis (Fig. 1b and **Supplementary Movie 1** online).

¹Department of Molecular Pharmacology, W200 Clark, 318 Campus Drive, Stanford University Medical School, Stanford, California 94305, USA. ²Department of Molecular Pharmacology & Department of Biochemistry, 269 Campus Drive, Stanford University Medical School, Stanford, California 94305, USA. ³Correspondence should be addressed to T.M. (tobias.meyer@stanford.edu).

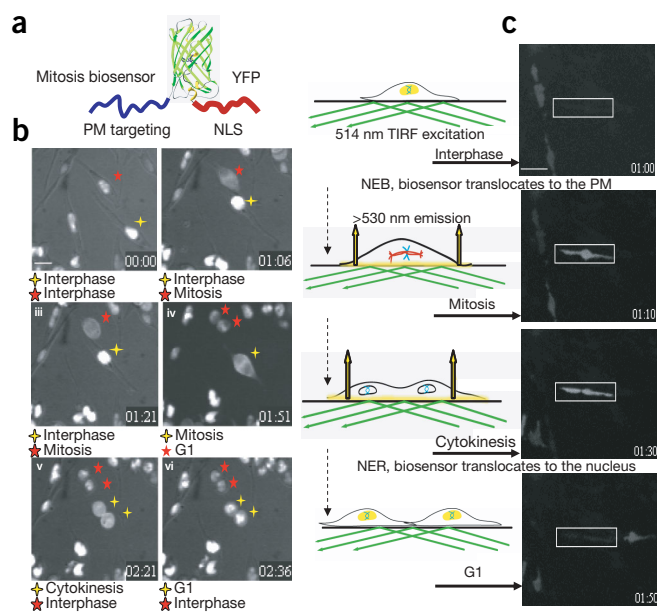


Figure 1 Design of the fluorescent mitosis biosensor. (a) A plasma membrane localization motif based on polybasic residues was added at the N terminus of a YFP-NLS construct. The structure of YFP was adapted²⁷. (b) Confocal images of RBL-FMB cells during interphase and mitosis (red and yellow stars mark individual cells) (see **Supplementary Movie 1** online). (c) Localization of the biosensor monitored by TIRF microscopy. Left, schematic representation of the mitosis monitoring system. The green arrows represent the light used for excitation of the mitosis biosensor, and the yellow arrows represent the fluorescence emission. Right, TIRF images of a RBL-FMB cell in the corresponding cell cycle phase (see **Supplementary Movie 2** online). The time (h:min) is in the lower right hand corner. Scale bars, 20 μ m.

Location of the biosensor monitored by TIRF microscopy

To determine if the change in fluorescence at the membrane could be monitored by TIRF microscopy, we adapted the same live-cell imaging setup used in the confocal experiments to a prism-based cyan fluorescent protein (CFP)/YFP TIRF system (Fig. 1c and **Supplementary Movie 2** online). During interphase, no substantial plasma membrane fluorescence was measured with TIRF. However, after NEB there was a large increase in plasma membrane fluorescence (Fig. 1c and **Supplementary Movie 2** online). This fluorescence was maintained until the nuclear envelopes of the two daughter cells reformed and the biosensor translocated back into the nucleus. Translocation into the nucleus was paralleled by a rapid loss in plasma membrane fluorescence, as measured by TIRF (Fig. 1c and **Supplementary Movie 2** online). Because the biosensor was monitored by the less toxic TIRF microscopy, we were able to take images at a rate of up to 2 images per minute, compared to every 5 min with epifluorescence

imaging and 15 with confocal imaging, thus greatly increasing the temporal resolution (Fig. 1b,c and **Supplementary Movies 1** and **2** online). Similarly, because the biosensor was only excited for approximately 30 min (when the cells are in mitosis), during the experiments we saw no substantial bleaching of the YFP.

Monitoring many mitotic events using wide-field TIRF

These findings made it possible to use wide-field TIRF microscopy to monitor many mitotic events in the same experiment. **Figure 2a** shows two planes of a 5-h TIRF experiment that was recorded through a 10 \times objective in which 70 cells proceeded through mitosis (**Supplementary Movie 3** online). To analyze these traces, we measured background-subtracted fluorescence over time at each location where a mitotic event occurred. Typical examples of such individual traces are shown in **Figure 2b**. These results confirm that the time period between NEB and NER can indeed be measured from the TIRF signal, enabling an accurate quantification of the duration of mitosis.

Detecting NEB, anaphase and NER with the mitosis biosensor

In 58 of the 70 cells (83%) that went through mitosis in the experiment, we noted a second smaller increase in plasma membrane fluorescence 6 to 12 min before the decrease in plasma membrane fluorescence (NER). Because previous studies in HeLa cells showed that anaphase onset occurs approximately 8 min before nuclear import is reactivated¹², we hypothesized that the second smaller increase in the TIRF signal was a reflection of anaphase onset. We addressed this by simultaneously monitoring plasma membrane fluorescence with TIRF and cell morphology with transmitted light (Fig. 2c and **Supplementary Movie 4** online). Consistent with the hypothesis, anaphase onset occurred immediately preceding the second marked increase of plasma membrane fluorescence that lasted until NER when the probe started to translocate back into the nucleus. This same correlation was observed in 11 out of the 15 cells (73%) monitored at this higher resolution. One explanation for the observed second increase in fluorescence intensity at anaphase is that the cells are moving closer to the adhesion surface. Another possibility is that the membrane interaction of the biosensor increases during anaphase, and the resulting increased membrane translocation causes the fluorescence increase. Regardless of the mechanism, the second peak of the fluorescence intensity trace provides a useful measurement of the time between anaphase onset and NER.

Figure 2d and **Table 1** show a detailed analysis of three independent experiments in which we tracked 217 mitotic events. We found that the mitosis is executed in these cells with great consistency. In 80% of the cells, the timing of mitosis fell between 26 and 38 min. To be precise, this measures the onset of prometaphase where NEB occurs and the end of telophase where the nuclear import machinery is reactivated. Even though these experiments were measured on different days with different cell preparations, the mean mitotic clock time was consistently 32 min. When the intensity traces showed the second spike in plasma membrane fluorescence, ($n = 152$, 70% of cells), the mean time between NEB and anaphase was 23 ± 7 min and the mean time between anaphase and NER was 8 ± 2 min. These results show that the mitotic machinery in these cells has a marked precision and consistency in keeping time even in unsynchronized cell cultures. These data also show the reproducibility of the TIRF-based

Table 1 Fidelity of the TIRF-based mitosis monitoring system

Expt.	NEB-NER					NEB-anaphase					Anaphase-NER				
	No.	Med.	Ave.	S.d.	S.e.m.	No.	Med.	Ave.	S.d.	S.e.m.	No.	Med.	Ave.	S.d.	S.e.m.
1	70	30	31.9	7.6	0.9	58	22	24.5	8.2	1.1	58	8	8.0	2.1	0.3
2	69	30	31.3	6.0	0.7	49	22	22.7	4.7	0.7	49	8	8.0	2.0	0.3
3	78	30	31.7	7.4	0.8	45	22	23.5	6.9	1.0	45	8	8.0	2.3	0.3

Data from three experiments taken on three different days are shown. All units are minutes with the exception of cell number. No., cell number; Med., median; Ave., average; s.d., standard deviation; s.e.m., standard error of the mean.

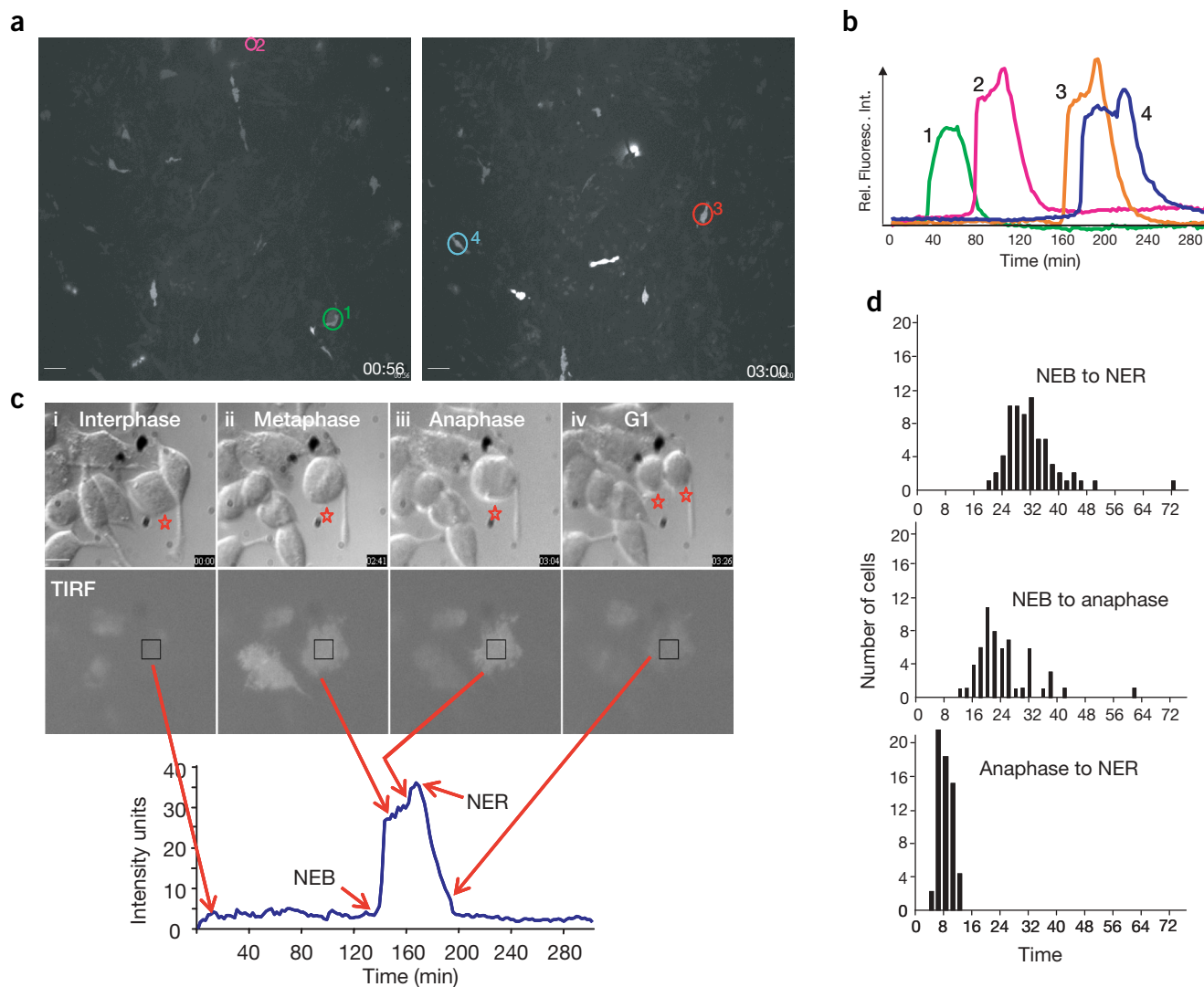


Figure 2 Monitoring multiple mitotic events in one experiment. **(a)** Two frames from a 5-h wide-field TIRF time-lapse experiment. Circles represent a location where a cell underwent mitosis. See **Supplementary Movie 3**. The time (h:min) is in the lower right hand corner. Scale bar, 50 μm . **(b)** Plots of fluorescence intensity versus time for the four corresponding cells circled in **a**. **(c)** RBL-FMB cells were imaged in parallel with TIRF (lower panels) and transmitted light (upper panels) microscopy through a 40 \times objective. The red stars in the transmitted light images mark the monitored cell. The region used to quantify the membrane fluorescence is shown in the TIRF images. The corresponding time point on the fluorescence intensity trace is shown below with a red arrow. See **Supplementary Movie 4**. Scale bars, 10 μm . **(d)** The time between NEB to NER, NEB to anaphase, and anaphase to NER was measured from the intensity traces obtained in the experiment represented in **a**.

method to monitor mitosis, as well as a substantial improvement in the ability to monitor more mitotic events in much less time.

Taxol has a graded effect on mitotic timing

Given this precision in mitotic timing, we wanted to learn whether sub-maximal doses of the mitosis inhibitor Taxol (paclitaxel) would have either a graded or an all-or-none effect on delaying the exit from mitosis. Taxol is a potent broad-spectrum anticancer agent that is particularly useful in the treatment of ovarian, breast and lung carcinomas¹³. It acts by binding and stabilizing microtubules, which results in mitotic arrest^{13–16}. Immunofluorescence studies in HeLa cells suggested that Taxol has a microtubule stabilization effect in the nanomolar concentration range¹⁴. Owing to the sensitivity of the TIRF-based mitosis monitoring system, we were able to see a significant increase in the time elapsed between NEB and NER, from an

average of 31.8 min to 35.6 min ($P = 0.014$) when concentrations of Taxol as low as 10 pM were applied to the cells (Fig. 3a and **Supplementary Table 1** online). This mitotic time increased as more Taxol was added until the cells arrested for the duration of the experiment at 10 nM (Fig. 3a and **Supplementary Table 1** online). In traces where it was possible to monitor the time elapsed between NEB and anaphase, the pre-checkpoint mitosis phase was substantially prolonged whereas the post-checkpoint anaphase to NER phase showed smaller and ungraded effects (**Supplementary Table 1** online).

We used conventional immunofluorescence experiments with the same RBL-FMBs¹³ as a control to confirm that the percentage of mitotic cells increased at higher Taxol concentrations¹⁴. RBL-FMB cells were treated with Taxol at varying doses for 20 h, fixed and stained with an antibody that recognizes alpha-tubulin and the DNA stain Hoechst 33342 (Molecular Probes) (Fig. 3b). With these two

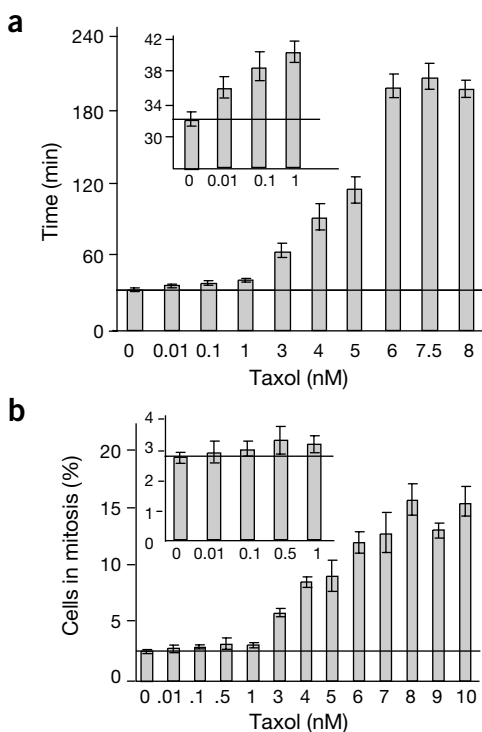


Figure 3 The effect of the cancer therapeutic Taxol on mitotic timing. (a) Taxol was added at the stated dose to the perfusion medium and cells were monitored as described in Fig. 2. Plotted are the average time between NEB and NER with the black line representing the average time between NEB and NER of untreated cells. The inset is a plot of the lower concentrations of Taxol studied. (b) Taxol concentration dependence for mitotic arrest. The black line represents the percentage of mitotic cells in untreated cells. The inset is a plot of the lower concentrations of Taxol studied. See **Supplementary Table 1** for detailed analysis.

stains mitotic spindles are easily recognized and the mitotic index can be quantified. Nevertheless, the effects at low Taxol concentrations went unseen in those experiments (Fig. 3b). Consistent with the first hypothesis, these results suggest that the mitotic clock is slowed down by Taxol in a graded way by delaying anaphase onset. Furthermore, these studies also highlight the sensitivity of this approach and how it can be used to measure small changes in the mitotic clock at clinically relevant drug concentrations.

Mad2 knockdown results in shortened but precise mitoses

Because the TIRF-based mitosis monitoring system was able to detect extremely subtle and graded effects of Taxol on the spindle checkpoint, we set out to determine whether this assay could detect if the checkpoint is engaged only when these RBL cells are perturbed or if it imposes a substantial delay on mitosis even in unsynchronized and unperturbed cells. The mitotic control system in these cells could function in two ways: (i) it could be driven by a fast internal mitotic timer that gets stopped during each cell cycle at the checkpoint and waits for a checkpoint release to continue or, (ii) by a checkpoint that only substantially delays the internal mitotic timer if the chromosome assembly is disrupted. Ptk1 cells entered anaphase 23 ± 1 min after the last kinetochore was attached to the spindle suggesting an active checkpoint in unperturbed cells¹⁷. When an antibody recognizing Mad2 was microinjected into either Ptk1 cells or primary human keratinocytes early in mitosis, the cells underwent premature anaphase

onset suggesting the spindle checkpoint plays an important role in the normal timing of mitosis¹⁸. We were able to directly address this issue by disabling the spindle checkpoint using RNAi to suppress the expression of Mad2 and observe any reduction in mitotic timing. Mad2, in conjunction with Bub1/Bub3, arrests cells in metaphase by inhibiting the ubiquitin ligase activity of the anaphase-promoting complex (APC), which is responsible for degrading securin^{4,19}. Mouse embryonic cells lacking Mad2 did not arrest at metaphase and the absence of this checkpoint resulted in chromosome missegregation, genetic instability and apoptosis^{5,20}. Studies of arrested cells suggested that a dominant negative Mad2 can induce precocious anaphase onset^{21,22}.

In three separate experiments we reduced the expression of rat Mad2 (rMAD2) by electroporating siRNAs processed by the RNase Dicer (d-siRNAs) into RBL-FMB cells²³. The resulting time in between NEB and NER was on average only 26.8, 25.9, 24.9 min compared to 32 min for control (firefly luciferase (GL3) d-siRNA) or untreated cells ($P = 0.00008$) (Fig. 4a,b and Table 2). As expected, the reduced time was a result of a decrease in the time elapsed between NEB and anaphase (Fig. 4c and Table 2). Mad2 protein knockdown was verified by western blot analysis (Fig. 4d). The measurements indicate that even a partial knockdown of Mad2 leads to full inactivation of the spindle checkpoint suggesting an all-or-none activation/inactivation mechanism via Mad2. Furthermore, these RNAi measurements directly demonstrate that Mad2 has a critical role in the spindle checkpoint as has been suggested previously by other approaches^{18,21,22}. These data confirm that the first hypothesis is correct and that during a normal cell cycle the spindle checkpoint imposes a marked delay onto the mitotic clock even in these relatively fast mitotic cells. Interestingly, because the TIRF-based mitosis monitoring system enabled us to analyze many cells, we were able to observe an internal mitotic timer that runs faster than the timer with a functional checkpoint, but is itself precise.

DISCUSSION

This study introduces a nonperturbing, genetically encoded, fluorescent reporter capable of monitoring mitosis in hundreds of cells in a single experiment. This biosensor repeatedly showed that the mitotic clock of unsynchronized RBL cells has a marked precision with 80% of cells completing mitosis in 32 ± 6 min. We also found significant ($P = 0.014$) delays in mitotic timing at concentrations of Taxol, an anti-cancer agent, that were 1% of the previous minimal effective doses. These results provide a plausible explanation of why Taxol is clinically active at low concentrations. Finally, inactivation of the checkpoint by targeting the regulator Mad2 with RNAi consistently shortened mitosis, providing direct evidence that the internal mitotic timing mechanism is much faster in cells that lack the spindle checkpoint.

This fluorescent mitotic biosensor can be used as a versatile tool in high content screening of small molecule and RNAi libraries. The throughput of the TIRF-based mitosis measurements can be increased by using a large area TIRF microscope developed recently that enables one to monitor thousands of cells at one time²⁴. For example, by using such a microscope and by spotting different cell populations on coverslips, the mitotic biosensor could easily be used to screen the effect on mitotic timing of libraries of expression constructs²⁵, RNAi libraries or putative cancer therapeutics. Similarly, we hope to increase the temporal resolution with more conventional microscopy methods by using cell lines that are more resistant to phototoxicity and by using free radical scavengers. The mitosis biosensor could then be used with currently available automated

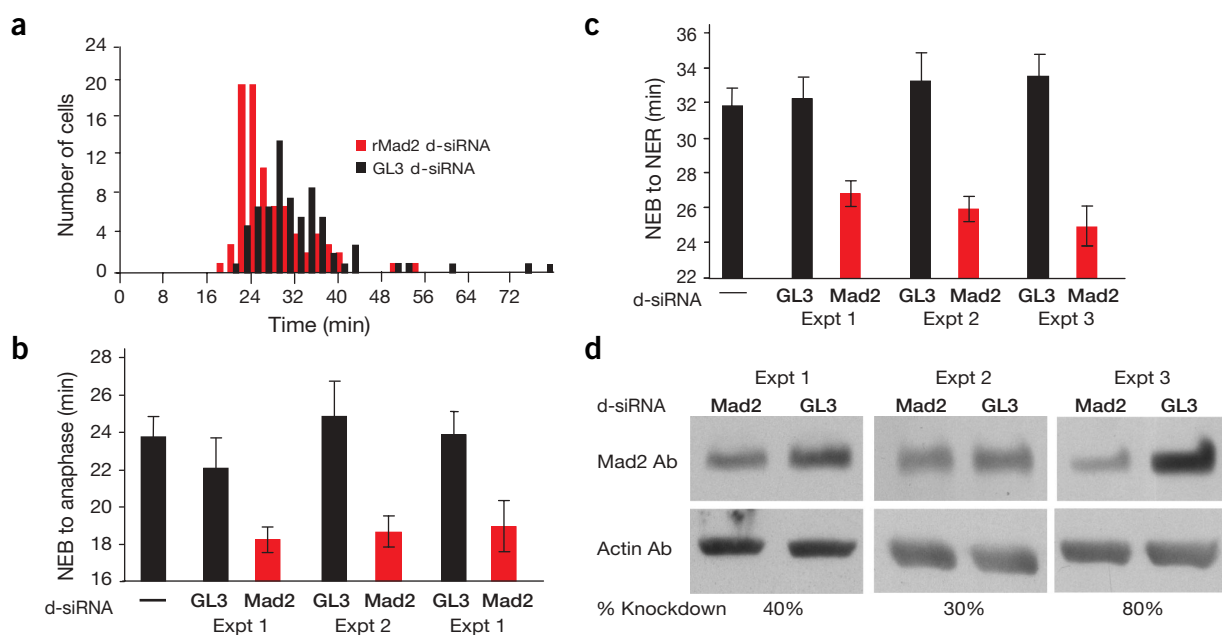


Figure 4 Knockdown of Mad2 with d-siRNA results in a shortened mitosis. RBL-FMB cells were transfected with d-siRNAs corresponding to the rMad2 gene, or firefly luciferase (GL3) control d-siRNAs and imaged 48 h later. **(a)** Histograms from experiment no. 1 (**Table 2**) comparing Mad2 d-siRNA treated-RBL-FMBs (red) and GL3-treated RBL-FMBs (black). **(b,c)** The time between NEB and NE from all three experiments is compared in **(b)** and NEB to anaphase in **(c)**. See **Table 2** for detailed analysis. **(d)** Western blot analysis of Mad2 expression in d-siRNA-treated RBL-FMB cells. RBL-FMB cells were transfected with d-siRNAs targeting Mad2 and the control firefly luciferase gene GL3. The cells were lysed 48 h after transfection and prepared for western blot analysis. Protein levels were normalized with an actin antibody.

live-cell imagers. Unlike fixed cell assays that can display gross mitotic defects, this assay enables one to measure the timing of mitotic phases, as well as more precisely interpret a particular mitotic defect. One can also readily imagine additional biosensors, based on red fluorescent protein²⁶ and CFP, that monitor the G0 exit, the G1/S transition or other cell cycle phases to be combined with the mitotic biosensor described here. In summary, live-cell fluorescent biosensors can serve as versatile and sensitive tools for measuring the precision of the mitotic clock and other cell cycle events, for dissecting the molecular control of mitotic timers and checkpoints, for high content screening and for understanding drug actions at clinically relevant concentrations.

METHODS

Engineering of the fluorescent mitosis biosensor, pFMB. We amplified 28 amino acids from the C terminus of the small GTPase Ras-like protein (Rit) from a CFP-Rit expression clone provided by Won Do Heo using the following primers: 5'-GCCG GCT AGC ATG GAG AAA AAA TCT AAG CCC AA-3'; 5'-GGC CAC CGG TCC AGT TAC TGA ATC TTT CTT CT-3'. The 5' primer used for PCR included a *NheI* site and the 3' primer included an *AgeI* site. These restriction digest sites were used to fuse the PCR product to the NH2 terminus of an EYFP targeted to the nucleus with a triplet repeat of the SV40 NLS (EYFP-NLS, Clontech).

Generation of rMad2 d-siRNAs. Rat Mad2 was isolated from an RBL cDNA library using the following primers: 5'-GCG TAA TAC GAC TCA CTA TAG

Table 2 Mitotic times are consistently reduced as a result of Mad2 knockdown

	NEB-NER					NEB-anaphase					Anaphase-NEB				
	No.	Med.	Ave.	S.d.	S.e.m.	No.	Med.	Ave.	S.d.	S.e.m.	No.	Med.	Ave.	S.d.	S.e.m.
Untreated	218	30	31.8	8.1	1.0	152	22	23.7	7.0	1.1	152	8	8.0	2.1	0.3
Expt. 1															
GL3 d-siRNA	74	30	32.2	10.2	1.2	51	20	22.1	10.4	1.6	51	8	8.9	2.7	0.4
Mad2 d-siRNA	86	26	26.8	6.5	0.7	39	17	18.2	4.7	0.7	39	8	7.9	2.8	0.4
Expt. 2															
GL3 d-siRNA	41	30	33.2	9.9	1.6	25	22	24.8	9.1	1.9	25	8	7.6	2.0	0.4
Mad2 d-siRNA	62	26	25.9	5.8	0.7	31	20	18.6	4.7	0.8	31	6	7.4	2.6	0.5
Expt. 3															
GL3 d-siRNA	43	32	33.5	7.7	1.2	17	24	23.8	5.8	1.3	17	8	7.4	1.8	0.4
Mad2 d-siRNA	38	24	24.9	6.6	1.1	23	18	18.9	6.6	1.4	23	8	7.8	1.9	0.4

Detailed analysis of three independent experiments in which RBL-FMB cells were transfected with d-siRNAs targeting Mad2 or firefly luciferase (GL3) as a control. The results are compared with the results obtained for untreated cells. All units are min with the exception of cell number. No., cell number; Med., median; Ave., average; s.d., standard deviation; s.e.m., standard error of the mean.

GAT GGC ACA GCA GCT CGC C CG-3'; 5'-GCG TAA TAC GAC TCA CTA TAG GTC AGT CAC TGA CAG GTG TTT-3' (T7 promoters are boldface). The resulting cDNA was transcribed *in vitro* to yield a 600 bp dsRNA. *In vitro* processing with Dicer enzyme was done as previously described²³.

Cell culture and transfections. RBL cells were grown in DMEM supplemented with 10% fetal calf serum, 2 mM glutamine, 100 U/ml penicillin and 100 µg/ml streptomycin (all from Invitrogen). Ten million cells were electroporated (BioRad) in 600 µl of medium with 40 µg of pFMB. These were allowed to recover for 48 h and cells stably expressing the biosensor were selected for by the addition of 1 µg/ml Geneticin (Invitrogen). Ten days after the addition of Geneticin, the cells were sorted based on EYFP fluorescence using FACS.

Transfection of the d-siRNAs was done as follows. We incubated 750,000 cells in cytomix buffer (25 mM HEPES (pH 7.6), 120 mM KCl, 10 mM K₂HPO₄, 5 mM MgCl₂, 0.15 mM CaCl₂, 2 mM EGTA, 1.9 mM ATP, 4.7 mM glutathione), 10 µg of ECFP (Clontech), pGL3 (Promega) and 1 µg of the relevant d-siRNA for 10 min at 22 °C while shaking. The cells were electroporated with an ECM 830 square wave, 8-well electroporator (BTX). Cells were immediately plated onto a 25 mm, no. 2 coverslip and allowed to recover for 48 h before imaging or lysing for western blot analysis.

Confocal and TIRF microscopy. The localization of the mitosis biosensor was investigated by using a CFP/YFP custom-built spinning disc confocal microscope. An argon-ion laser (120 mW; Melles Griot) provided 514-nm light for excitation of the biosensor. Laser light homogenized with a rotating diffuser (Physical Optics) was coupled into a Yokogawa spinning disc head (Perkin Elmer) mounted on an Olympus microscope. Exposure of the RBL-FMBs to laser light was controlled by a Sutter Lambda 10-2 filter wheel (Sutter Instrument). Emitted light was detected with a 530-nm long pass interference filter (Chroma Technology) mounted in a Sutter Lambda 10-2 filter wheel (Sutter Instrument). Images were captured every 15 min with an Orca II cooled CCD camera (Hamamatsu). The shutters, filter wheel and camera were controlled by Metamorph software (Universal Imaging).

TIRF microscopy was carried out as described previously¹¹. Briefly, an argon-ion laser provided 514-nm laser light for excitation of the biosensor (Lexcel Laser). Exposure of the RBL-FMBs to laser light was controlled by a Uniblitz shutter (Vincent). Laser light homogenized with a rotating diffuser (Physical Optics) was refocused onto a dove prism at an angle yielding total internal reflection (>61°C for a glass-water interface at 37 °C). The excitation light could also be redirected to the back of the microscope and down to the sample via appropriate dichroic mirrors (Chroma Technology) for epillumination. Fluorescence was recorded at 530 nm with bandpass interference filters (30–50 nm half-bandwidth; Chroma Technology) mounted in a Sutter Lambda 10-2 filter wheel (Sutter Instrument). Images were captured every 2 min with a cooled CCD camera (Micromax; Roper Scientific). The shutters, filter wheel and camera were controlled by Metamorph software (Universal Imaging).

Both systems were heated with an ASI 400 Air Stream Incubator (Nevtek). The cells were perfused with fresh growth medium saturated with 10% CO₂ that was heated with an inline solution heater (Warner Instruments).

Data analysis. Metamorph software (Universal Imaging) was used for data image analysis. Fluorescence intensity was recorded over the entire stack of images by drawing regions of interest over each mitotic cell. Background correction was done by subtracting the intensity of a background region of identical size next to each cell to account for the somewhat uneven background in the field of view over the time of the data collection. Background-corrected intensity values were exported to a Microsoft Excel file and plotted. NEB was determined as the time just before the dramatic increase in fluorescence intensity. Anaphase onset is defined as the time point immediately preceding the second smaller increase in fluorescence. NER was determined as the point in time when fluorescence intensity starts to fall back to baseline levels.

Immunofluorescence. Mitotic index was determined as previously described¹⁴. Briefly, 15,000 RBL-FMB cells plated in 8-well Labtek chambers (Nalge Nunc) and exposed to paclitaxel (Sigma Aldrich) for 20 h. The cells

were fixed and permeabilized with –20 °C cold methanol for 5 min at –20 °C. They were blocked with 10% fetal calf serum in PBS for 10 min at 22 °C. Alpha-tubulin was detected with a mouse monoclonal antibody clone GTU-88 (Sigma Aldrich). DNA was stained with Hoechst 33342 (Molecular Probes). Only cells that were clearly in metaphase or anaphase were counted as a percentage of the total. The cells were imaged with a Zeiss epifluorescence microscope (Carl Zeiss).

Western blot analysis. Cells were lysed 48 h after transfection with the d-siRNAs by vortexing in cold lysis buffer (0.42 M NaCl, 100 mM Tris, pH 7.9, 0.5% Triton X-100, 1 mM EDTA, 1 mM EGTA) supplemented with protease inhibitors (aprotinin 1 µg/ml, 0.2 mM phenylmethylsulfonyl fluoride, pepstatin, leupeptin and chymostatin, all at 0.2 µg/ml). Lysates were subjected to SDS-PAGE and transferred to polyvinylidene difluoride. Blots were probed with anti-Mad2 (1:1,000), or anti-actin (1:400, Santa Cruz). Secondary antibodies conjugated to horseradish peroxidase (HRP; Amersham) were used at 1:2,500. The Immuno-Star HRP chemiluminescent detection kit (Bio-Rad) was used for HRP detection. Films were scanned and protein level was quantified using Adobe Photoshop (Adobe). Regions of the same size were drawn around the bands corresponding to Mad2 and the background-subtracted average intensities were recorded. These data were normalized for protein amount with the actin band intensities. Mad2 protein levels were compared in cells treated with the Mad2 d-siRNA or the control GL3 d-siRNA.

Note: Supplementary information is available on the Nature Biotechnology website.

ACKNOWLEDGMENTS

We would like to thank Guowei Fang, Thierry Galvez, Marc Fivaz and Angie Hahn for critical reading of the manuscript. We would also like to thank G. Fang for his kind gift of the Mad2 antibody, Tom Wehrman for help with creating the stable line and the Meyer and Ferrell labs for their support. This work was supported by the National Institutes of Health.

COMPETING INTERESTS STATEMENT

The authors declare that they have no competing financial interests.

Received 24 September; accepted 2 December 2003

Published online at <http://www.nature.com/naturebiotechnology/>

- Ekholm, S.V., Zickert, P., Reed, S.I. & Zetterberg, A. Accumulation of cyclin E is not a prerequisite for passage through the restriction point. *Mol. Cell. Biol.* **21**, 3256–3265 (2001).
- Elledge, S.J. Cell cycle checkpoints: preventing an identity crisis. *Science* **274**, 1664–1672 (1996).
- Musacchio, A. & Hardwick, K.G. The spindle checkpoint: structural insights into dynamic signalling. *Nature Rev. Mol. Cell Biol.* **3**, 731–741 (2002).
- Yu, H. Regulation of APC-Cdc20 by the spindle checkpoint. *Curr. Opin. Cell Biol.* **14**, 706–714 (2002).
- Michel, L.S. *et al.* MAD2 haplo-insufficiency causes premature anaphase and chromosome instability in mammalian cells. *Nature* **409**, 355–359 (2001).
- Rieder, C.L. & Khodjakov, A. Mitosis through the microscope: advances in seeing inside live dividing cells. *Science* **300**, 91–96 (2003).
- Bajer, A. Cine-Micrographic Studies on mitosis in endosperm. *Exp. Cell Res.* **14**, 245–256 (1958).
- Rieder, C.L. Effect of hypothermia (20–25 degrees C) on mitosis in PtK1 cells. *Cell Biol. Int. Rep.* **5**, 563–573 (1981).
- Zhang, J., Campbell, R.E., Ting, A.Y. & Tsien, R.Y. Creating new fluorescent probes for cell biology. *Nat. Rev. Mol. Cell Biol.* **3**, 906–918 (2002).
- Steyer, J.A. & Almers, W. A real-time view of life within 100 nm of the plasma membrane. *Nat. Rev. Mol. Cell Biol.* **2**, 268–275 (2001).
- Tengholm, A., Teruel, M.N. & Meyer, T. Single cell imaging of PI3K activity and glucose transporter insertion into the plasma membrane by dual color evanescent wave microscopy. *Science's Stake* **2003**, PL4 (2003).
- Haraguchi, T. *et al.* Live fluorescence imaging reveals early recruitment of emerin, LBR, RanBP2, and Nup153 to reforming functional nuclear envelopes. *J. Cell Sci.* **113**, 779–794 (2000).
- Wang, T.H., Wang, H.S. & Soong, Y.K. Paclitaxel-induced cell death: where the cell cycle and apoptosis come together. *Cancer* **88**, 2619–2628 (2000).
- Jordan, M.A., Toso, R.J., Thrower, D. & Wilson, L. Mechanism of mitotic block and inhibition of cell proliferation by taxol at low concentrations. *Proc. Nat. Acad. Sci. USA* **90**, 9552–9556 (1993).
- Jordan, M.A. *et al.* Mitotic block induced in HeLa cells by low concentrations of paclitaxel (Taxol) results in abnormal mitotic exit and apoptotic cell death. *Cancer Res.* **56**, 816–825 (1996).
- Sorger, P.K., Dobles, M., Tournebise, R. & Hyman, A.A. Coupling cell division and cell death to microtubule dynamics. *Curr. Opin. Cell Biol.* **9**, 807–814 (1997).

17. Rieder, C.L., Schultz, A., Cole, R.W. & Sluder, G. Anaphase onset in vertebrate somatic cells is controlled by a checkpoint that monitors sister kinetochore attachment to the spindle. *J. Cell Biol.* **127**, 1301–1310 (1994).
18. Gorbsky, G.J., Chen, R.H. & Murray, A.W. Microinjection of antibody to Mad2 protein into mammalian cells in mitosis induces premature anaphase. *J. Cell Biol.* **141**, 1193–1205 (1998).
19. Fang, G., Yu, H. & Kirschner, M.W. The checkpoint protein MAD2 and the mitotic regulator CDC20 form a ternary complex with the anaphase-promoting complex to control anaphase initiation. *Genes Dev.* **12**, 1871–1883 (1998).
20. Dobles, M., Liberal, V., Scott, M.L., Benezra, R. & Sorger, P.K. Chromosome missegregation and apoptosis in mice lacking the mitotic checkpoint protein Mad2. *Cell* **101**, 635–645 (2000).
21. Mikhailov, A., Cole, R.W. & Rieder, C.L. DNA damage during mitosis in human cells delays the metaphase/anaphase transition via the spindle-assembly checkpoint. *Curr. Biol.* **12**, 1797–1806 (2002).
22. Canman, J.C., Salmon, E.D. & Fang, G. Inducing precocious anaphase in cultured mammalian cells. *Cell Mot. Cyto.* **52**, 61–65 (2002).
23. Myers, J.W., Jones, J.T., Meyer, T. & Ferrell, J.E. Recombinant Dicer efficiently converts large dsRNAs into siRNAs suitable for gene silencing. *Nat. Biotechnol.* **21**, 324–328 (2003).
24. Teruel, M.N. & Meyer, T. Parallel single-cell monitoring of receptor-triggered membrane translocation of a calcium-sensing protein module. *Science* **295**, 1910–1912 (2002).
25. Heo, W.D. & Meyer, T. Switch-of-function mutants based on morphology classification of ras superfamily small GTPases. *Cell* **113**, 315–328 (2003).
26. Campbell, R.E. *et al.* A monomeric red fluorescent protein. *Proc. Nat. Acad. Sci. USA* **99**, 7877–7882 (2002).
27. Rekas, A., Alattia, J.R., Nagai, T., Miyawaki, A. & Ikura, M. Crystal structure of venus, a yellow fluorescent protein with improved maturation and reduced environmental sensitivity. *J. Biol. Chem.* **277**, 50573–50578 (2002).